THE EFFECT OF SYMMETRIC AND ASYMMETRIC DYNAMICS ON PERIOD-N BIFURCATIONS

Andrew Honeycutt and Tony L. Schmitz
Department of Mechanical Engineering and Engineering Science
University of North Carolina at Charlotte, Charlotte, NC

INTRODUCTION

The mean material removal rate (MRR) in milling is calculated from the product of radial depth of cut, *a*, axial depth of cut, *b*, feed per tooth, f_t, and spindle speed, Ω. Because higher MRR reduces machining time, increasing MRR also decreases production cost. It is therefore desirable to increase all four process parameters (*a*, *b*, f_t, and Ω) within the limits of the machining system. Limitations to these increases include: chatter (or unstable machining performance), tool wear, torque/power limits for the selected spindle, and feed rate limits for the selected drive. While all four limits can be imposed individually (or in combination), the focus for this study is chatter.

It is well understood that chatter occurs due to the inherent combination of structural flexibility and the periodic cutting force that excites the structural dynamics. Two primary categories for unstable behavior are: 1) regenerative; and 2) mode coupling chatter. Only regenerative chatter, where the process feedback leads to gain-dependent behavior, is considered here. This feedback occurs because the instantaneous chip thickness depends on both the vibration state of the cutter at the current time and the surface left behind by previous tooth passages (which introduces a time delay, or memory, in the differential equations of motion). Because the cutting force is a function of this instantaneous chip thickness and the current vibration state depends on the instantaneous force, the feedback loop is closed. Traditionally, the system gain is described as the axial depth of cut for a selected radial depth. The spindle speed dictates the time delay so, together, the spindle-speed and axial depth offer the control parameters for milling [1].

Traditionally, regenerative chatter is considered to be a self-excited vibration and can be described as a secondary Hopf bifurcation (a bifurcation is a dramatic change in the dynamic state due to small modifications in the process parameters). The relationship between Ω and the limiting *b* value is typically presented in a stability map, or stability lobe diagram. Figure 1 provides an example.

In recent research, it has been demonstrated that different types of instability can occur in milling. Not only can secondary Hopf bifurcations be observed, it has also been shown that period-n (n = 2, 3, 4, …) bifurcations can exist, where the system response repeats every n tooth periods (rather than every tooth period for the forced vibration that characterize stable milling) [2-3]. Figure 2 displays an example.

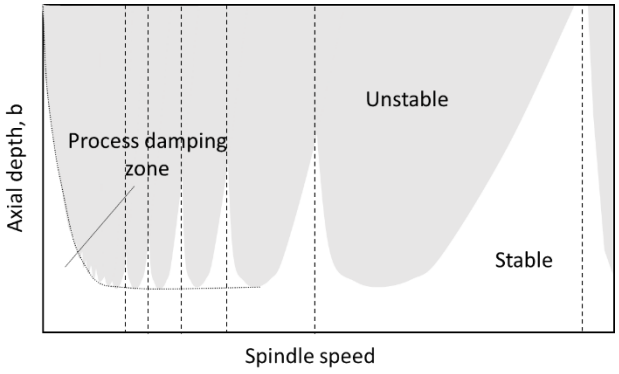

Figure 1. Example stability map for milling.

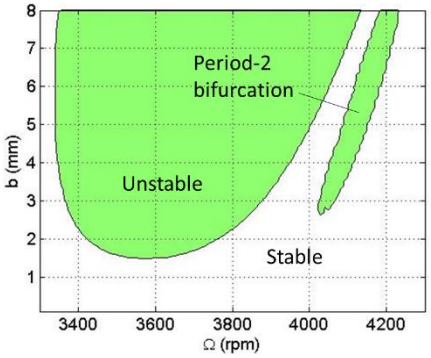

Figure 2. Stability map with period-2 bifurcation zone.

The purpose of this study is to experimentally and numerically (time domain simulation) explore the stability behavior for dynamic systems with both asymmetric and symmetric dynamics. Results are presented for a flexure-based experimental setup that produces significant asymmetry in the dynamic stiffness relative to the cutting direction. Period-n bifurcations are simulated and validated. Systems with symmetric dynamics that apply the same modal parameters as the flexible direction for the flexure-based setup are then simulated. Both period-n and secondary Hopf bifurcations are identified and compared to the asymmetric system behavior. Conclusions are finally presented.

ASYMMETRIC DYNAMICS

Because flexure-based experiments, where the workpiece is mounted on a single degree-of-freedom (SDOF) flexure, provide convenient measurement of the milling process outputs, they are a common choice for model validation. This setup represents the case of strongly asymmetric system dynamics because the SDOF flexure is much more flexible in one Cartesian direction than the other two. Additionally, the tool point dynamics are typically selected so that the tool's lowest dynamic stiffness is much higher than the flexure's lowest dynamic stiffness.

To demonstrate bifurcation behavior for a strongly asymmetric system, the milling response was predicted using time domain simulation and validated using the flexure-based experimental configuration shown in Figure 3. For this setup, the flexure's time dependent displacement, velocity, and acceleration during cutting were measured by a capacitance probe, laser vibrometer, and low mass accelerometer, respectively, to assess milling behavior under various process parameters. The laser tachometer signal was used to synchronously sample the flexure motion data.

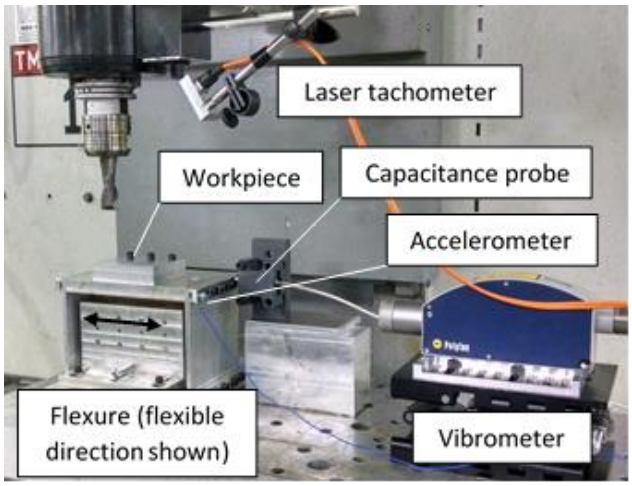

Figure 3. SDOF parallelogram, leaf-type flexure experimental setup.

The flexure and tool point dynamics are listed in Table 2. These modal parameters were extracted from *x* (feed) and *y* direction impact tests completed on both the flexure and single-flute 19.05 mm diameter, 30 deg helix endmill. The mechanistic cutting force coefficients for the 6061-T6 aluminum workpiece were k_{tc} = 792 N/mm^2, k_{nc} = 352 N/mm^2, k_{te} = 26 N/mm, and k_{ne} = 28 N/mm. Time domain simulations were completed for up milling in the flexure's low stiffness direction with a 2 mm radial depth and 0.1 mm/tooth feed. The simulation outputs included the cutting force and flexure motion *x* and *y* components for a range of {spindle speed, axial depth} combinations. The flexure displacement and velocity signals were synchronously sampled at the tooth period (once-per-revolution for the single flute cutter). Figure 4 shows the flexure's time dependent, feed direction displacement, *x*, and velocity, *dx/dt*, as well the periodic sampling result (circles). It is observed that the process behavior repeats each period for the stable {3400 rpm, 6 mm axial depth} cut after the initial transients have attenuated.

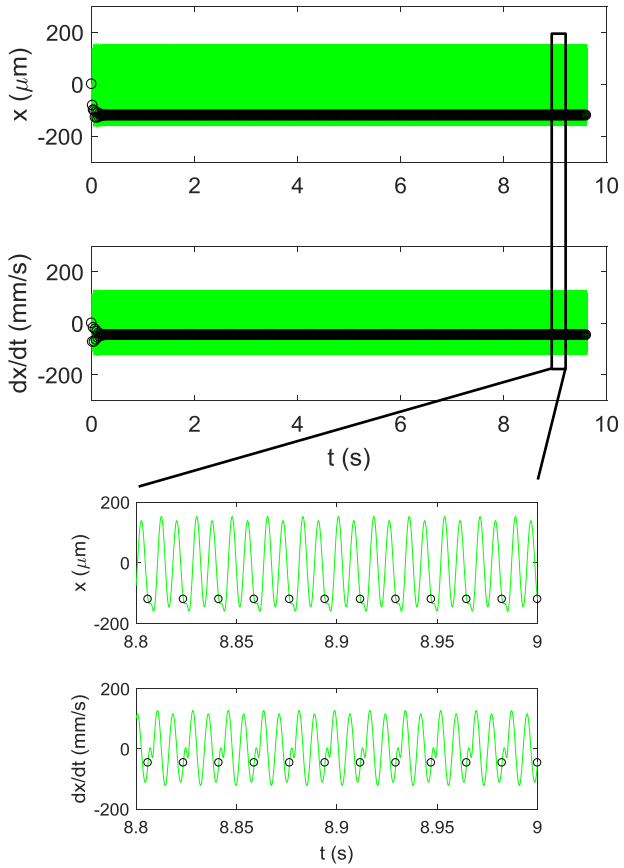

Figure 4. Predictions for stable {3400 rpm, 6 mm axial depth} up milling using the Table 1 dynamics with a 2 mm radial depth and 0.1 mm/tooth feed. (Top) time dependent displacement with periodic samples (circles); (bottom) time dependent velocity with periodic samples. (Inset) higher magnification view to observe individual periodic samples of the displacement (top) and velocity (bottom).

Table 1. Modal parameters (natural frequency, dimensionless viscous damping ratio, and stiffness) for asymmetric flexible feed direction experimental setup.

Flexure			Tool point		
x (feed direction)			*x*		
130.0 Hz	0.0147	2.1×10^6 N/m	1055 Hz	0.045	4.2×10^7 N/m
y			*y*		
756 Hz	0.085	7.7×10^7 N/m	1055 Hz	0.045	4.2×10^7 N/m

To more effectively visualize the process behavior, the displacement is plotted versus the velocity in the Figure 5 Poincaré map. Here, the sampled points all align at a single location because the stable milling process exhibits forced vibration at the tooth period. For this figure, the transient portion (during the cut entry) was excluded to leave only the steady-state behavior.

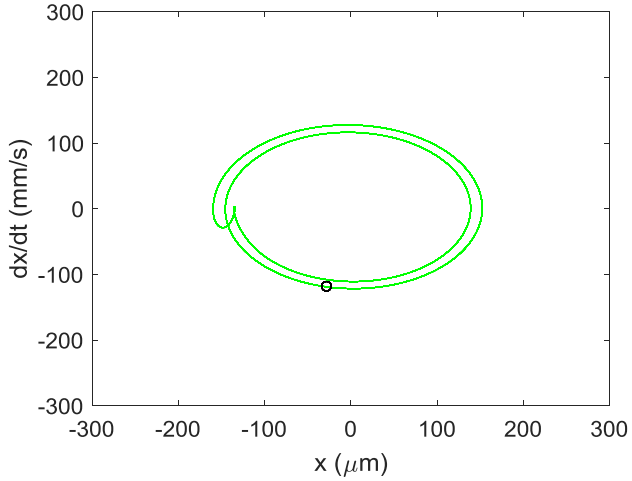

Figure 5. Predicted Poincaré map for stable {3400 rpm, 6 mm axial depth} up milling using the Table 1 dynamics with a 2 mm radial depth and 0.1 mm/tooth feed.

Figures 6 and 7 show the results for {3310 rpm, 6 mm axial depth}. This behavior represents a period-2 bifurcation because the motion repeats every other tooth period, rather than every tooth period. Here, two points are observed in the Poincaré map. Cutting tests were completed on the Figure 3 setup to validate the time domain predictions. The experimental results are presented in Figure 8, where the displacement was measured by the capacitance probe and the velocity by the laser vibrometer. The time dependent signals were sampled once per tooth period using the laser tachometer signal and the transients (from the cut entry) were excluded. Good agreement with Figure 7 is observed and the simulation performance is verified.

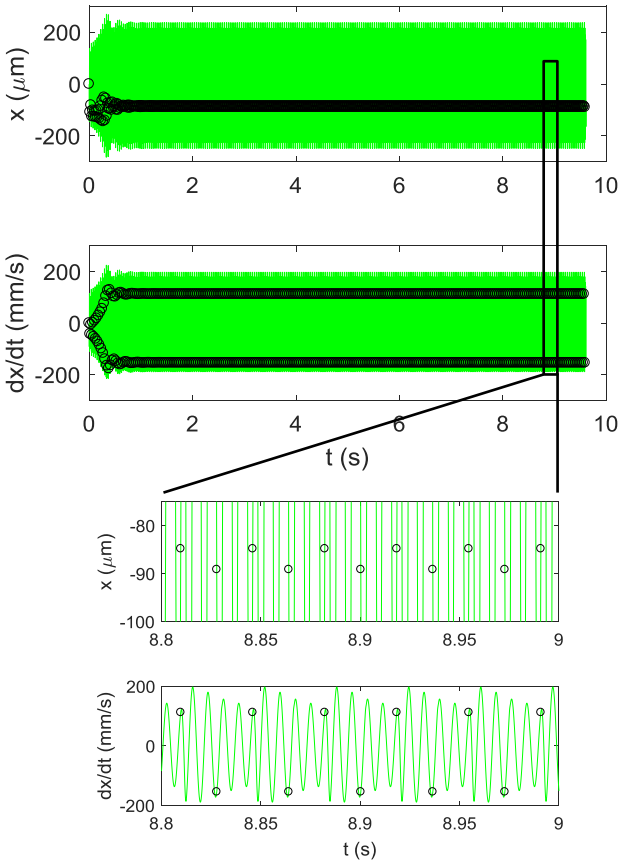

Figure 6. Predictions for period-2 {3310 rpm, 6 mm axial depth} up milling using the Table 1 dynamics with a 2 mm radial depth and 0.1 mm/tooth feed.

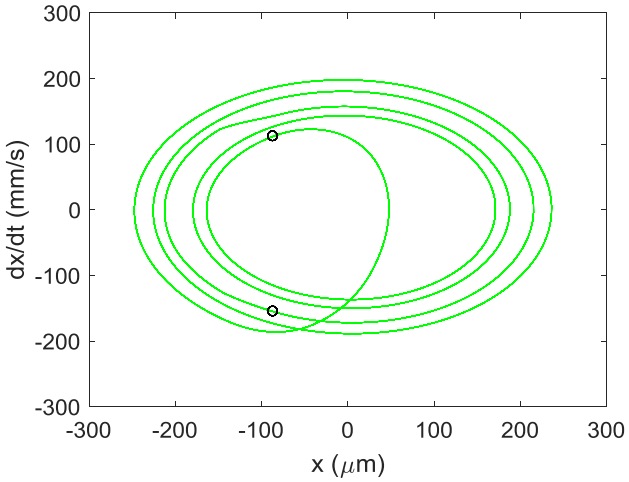

Figure 7. Predicted Poincaré map for period-2 {3310 rpm, 6 mm axial depth} up milling using the Table 1 dynamics with a 2 mm radial depth and 0.1 mm/tooth feed.

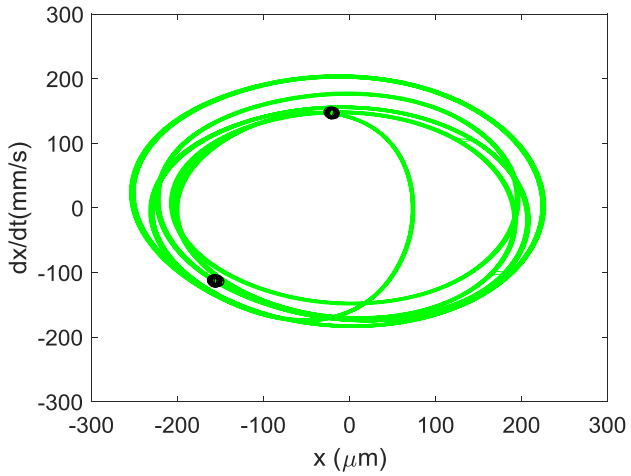

Figure 8. Experimental Poincaré map for period-2 {3310 rpm, 6 mm axial depth} up milling using the Table 1 dynamics with a 2 mm radial depth and 0.1 mm/tooth feed.

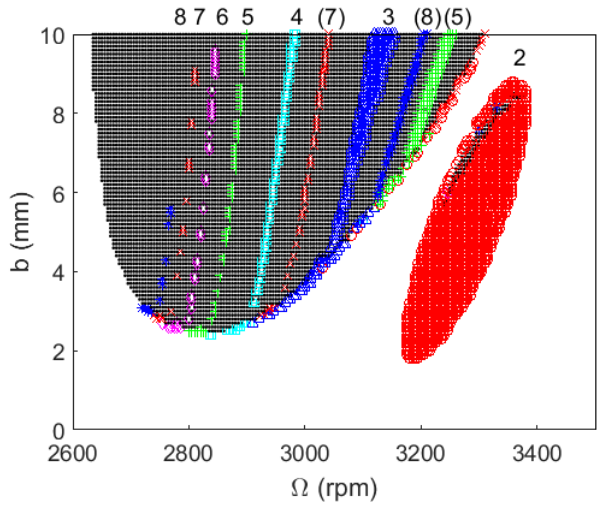

Figure 9. Predicted stability map for up milling using the Table 1 dynamics with a 2 mm radial depth and 0.1 mm/tooth feed. The bifurcation period is identified by the numerals 2-8.

To obtain a global stability map, time domain simulations were completed over a grid of spindle speeds, Ω, from 2600 rpm to 3500 rpm (5 rpm increments) and axial depths, *b*, from 0.1 mm to 10 mm (0.1 mm increments). Periodic sampling was applied to the *x* data to individually identify period-2 through period-8 bifurcations. The results are presented in Figure 9, where the symbols are defined in Table 2. An elliptical, period-2 "island" is seen between 3200 rpm and 3400 rpm within the stable zone; the Figure 7 prediction and Figure 8 experiment were completed at a point inside this island. Period-2 through period-8 bifurcation "bands" are also observed within the secondary Hopf bifurcation zone (i.e., traditional regenerative chatter). In Figure 9, the bifurcation period is identified using the numbers 2-8, which appear at decreasing spindle speeds (i.e., right to left from 2 to 8). Repeated bands at higher speeds are also present; these are indicated with parentheses (e.g., (7) appears between 3 and 4 at a higher spindle speed range than 7).

Table 2: Symbols for period-n stability maps.

Period	Symbol	Color
2	Circle	Red
3	^	Blue
4	Square	Cyan
5	+	Green
6	Diamond	Magenta
7	×	Red
8	*	Blue
Stable	No symbol	(White space)
Secondary Hopf	·	Black

Using Figure 9, various bifurcation behaviors can be identified and then studied individually. For example, a secondary Hopf bifurcation is observed at {2850 rpm, 6 mm axial depth}. This quasi-periodic behavior is displayed in Figure 10 (time domain) and Figure 11 (Poincaré map). In Figure 11, the characteristic elliptical distribution for the periodically sampled points is obtained due to the presence of the new incommensurate chatter frequency (i.e., self-excited vibration).

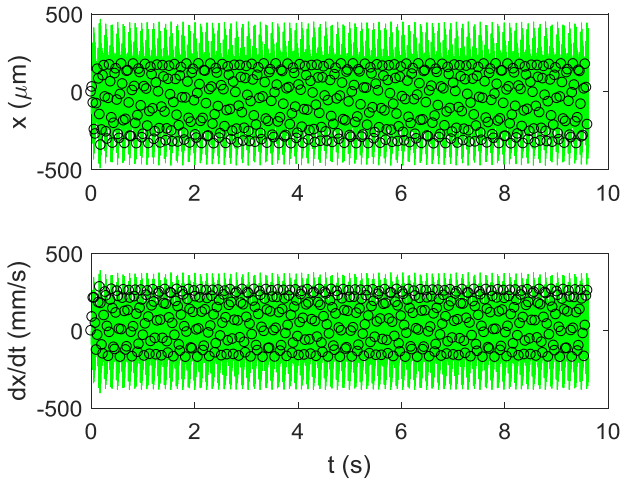

Figure 10. Predictions for unstable {2850 rpm, 6 mm axial depth} up milling using the Table 1 dynamics with a 2 mm radial depth and 0.1 mm/tooth feed.

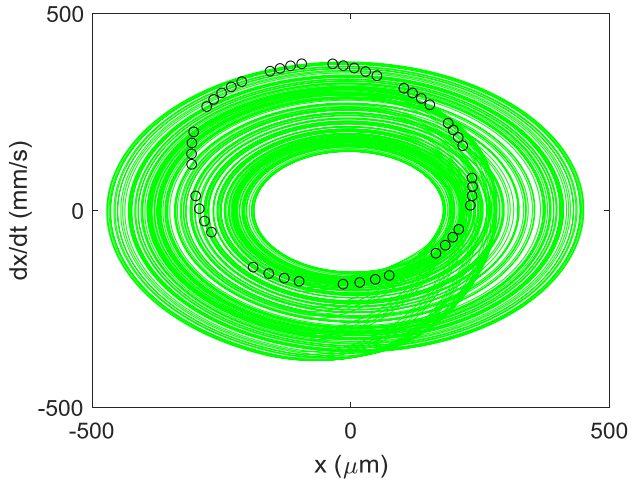

Figure 11. Predicted Poincaré map for unstable {2850 rpm, 6 mm axial depth} up milling using the Table 1 dynamics with a 2 mm radial depth and 0.1 mm/tooth feed.

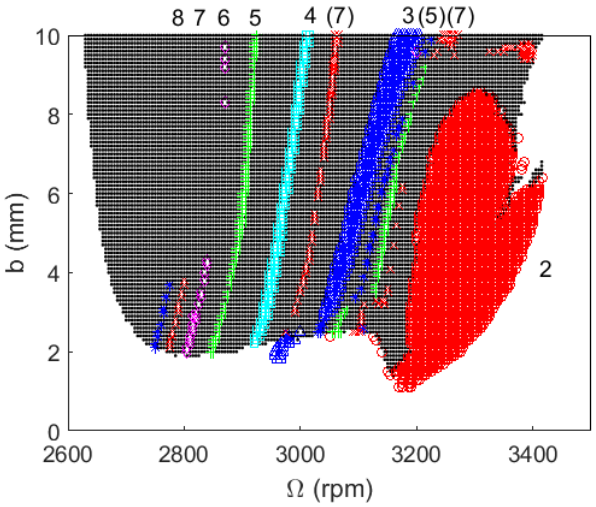

Figure 12. Predicted stability map for up milling using the Table 3 symmetric dynamics with a 2 mm radial depth and 0.1 mm/tooth feed.

SYMMETRIC DYNAMICS

Because tools, holders, and spindles are rotationally symmetric by design, it is common to observe symmetric system dynamics in practice. Therefore, simulations were next completed using the validated time domain solution to see how the process behavior changed with a shift from asymmetric to symmetric dynamics. First, the Table 1 dynamics were modified to match the flexure's stiff *y* direction modal parameters to the flexible *x* direction; see Table 3. The same cutting force model and cutting conditions as used for Figure 9 were applied. The symmetric dynamics stability map is provided in Figure 12 (5 rpm and 0.1 mm increments). It is seen that: 1) the period-2 island has expanded into the original secondary Hopf zone; and 2) a "hump" has appeared in the stability boundary near {3100 rpm, 2 mm axial depth}.

Table 3. Modal parameters (natural frequency, dimensionless viscous damping ratio, and stiffness) for strongly asymmetric flexible feed direction experimental setup.

Flexure			Tool point		
x (feed direction)			*x*		
130.0 Hz	0.0147	2.1×10^6 N/m	1055 Hz	0.045	4.2×10^7 N/m
y			*y*		
130.0 Hz	0.0147	2.1×10^6 N/m	1055 Hz	0.045	4.2×10^7 N/m

WEAKLY ASYMMETRIC DYNAMICS

As a final study, a dynamic system with weak asymmetry was considered. This is seen in practice, for example, when the flexible tool response dominates the system dynamics, but the *x* direction is slightly stiffer than the *y* (or vice versa) due to asymmetry in the spindle-machine dynamics into which the endmill is inserted. For this study, the *y* direction stiffness and natural frequency were set to 90% of the *x* (feed) direction values; see Table 4. The results are displayed in Figures 13 (symmetric) and 14 (asymmetric). It is seen that the Figure 14 stable gap (white space) has shifted, the period-2 island appears within the stable zone, and the stability hump has grown to a local stability peak (near 2900 rpm) with a new period-2 zone immediately to its left. Clearly, the weak asymmetry has added significant complexity to the overall stability behavior.

Table 4. Modal parameters for weakly asymmetric dynamics system (symmetric when no multiplier used for y direction).

Flexure			Tool point		
x (feed direction)			*x*		
125.8 Hz	0.0136	1.75×10^6 N/m	1188 Hz	0.095	4.24×10^7 N/m
y			*y*		
0.9(125.8) Hz	0.0136	0.9 (1.75×10^6) N/m	1188 Hz	0.095	4.24×10^7 N/m

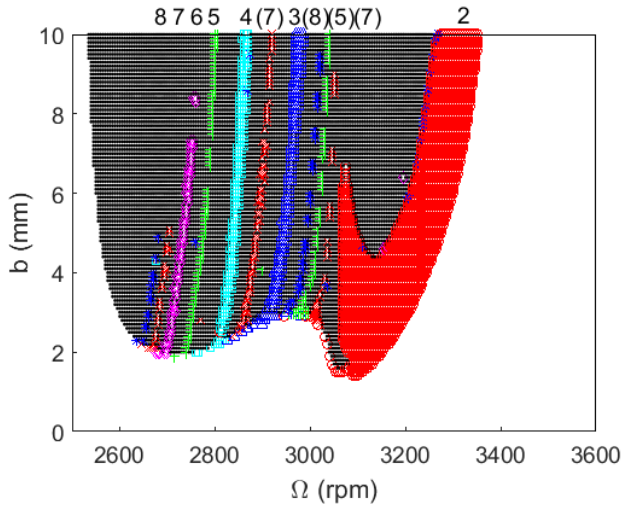

Figure 13. Predicted stability map for up milling using the symmetric Table 4 dynamics with a 2 mm radial depth and 0.35 mm/tooth feed.

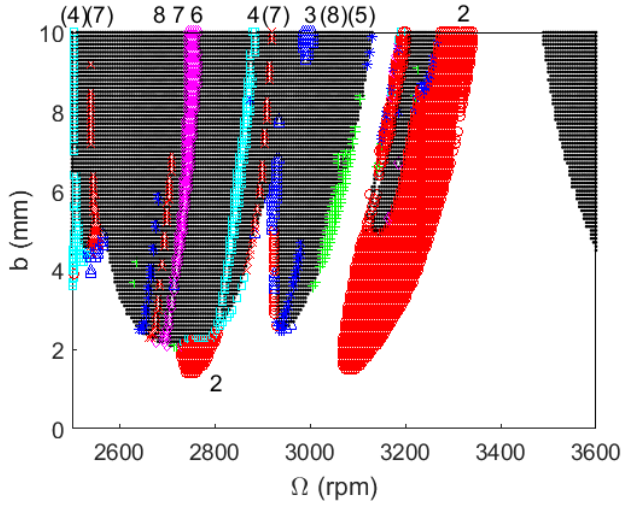

Figure 14. Predicted stability map for up milling using the asymmetric Table 4 dynamics with a 2 mm radial depth and 0.35 mm/tooth feed.

CONCLUSIONS

This paper described the application of time domain simulation to the prediction of milling behavior for asymmetric, symmetric, and weakly asymmetric system dynamics. These choices correspond to three common physical setups: a single degree-of-freedom flexure setup often used to perform validation experiments (asymmetric); long, flexible endmill dynamics (symmetric); and tool or workpiece-dominated dynamics with slight asymmetry in the plane of the cut (weakly asymmetric). The time domain simulation outputs included displacement and velocity, which were synchronously sampled to identify the milling behavior. The two signals were sampled at the tooth period to produce Poincaré maps. Also, subharmonic periodic sampling was completed at integer multiples of the tooth period and then these results were combined with a numerical stability metric to automatically produce a stability map from a grid of time domain simulations. Experimental validation was provided for the flexure-based setups. The following results were observed.

- Asymmetric dynamics

In a flexure-based setup (Table 1), the process behavior was predicted and verified for feed in the flexible direction of the asymmetric flexure. A period-2 island was seen in the stable zone with period-3 and higher bands located within the traditional secondary Hopf bifurcation zone.

- Symmetric dynamics

The dynamics for the flexure-based setup was modified to match both directions to the original flexible direction. Time domain simulations were completed to produce a stability map. It was seen that the period-2 island expanded into the original secondary Hopf zone and a hump appeared in the stability boundary near the new period-2 location in both instances. The period-3 and higher bands persisted.

- Weakly asymmetric dynamics

In this case, the stiff direction was similar to the flexible direction, but not identical (the stiffness and natural frequency were set to 90% of the flexible direction values). It was seen in the stability map that the stable gap shifted in spindle speed, a period-2 island appeared within the stable zone, and a new local stability peak with a corresponding period-2 zone appeared. Generally speaking, the weak asymmetry added significant complexity to the stability map.

ACKNOWLEDGEMENTS

This material is based on work supported by the National Science Foundation under Grant No. CMMI-1561221.

REFERENCES

[1] Schmitz, T. and Smith, K.S., Machining Dynamics: Frequency Response to Improved Productivity, Springer, New York, NY, 2009.

[2] Honeycutt, A. and Schmitz, T., 2016, A Numerical and Experimental Investigation of Period-n Bifurcations in Milling, Journal of Manufacturing Science and Engineering, 139/1: 011003.

[3] Honeycutt, A. and Schmitz, T., 2016, A New Metric for Automated Stability Identification in Time Domain Milling Simulation, Journal of Manufacturing Science and Engineering, 138/7: 074501.